

Cranial anatomy of *Bolotridon frerensis*, an enigmatic cynodont from the Middle Triassic of South Africa, and its phylogenetic significance

Luisa C. Pusch^{1,2}, Christian F. Kammerer^{3,4} and Jörg Fröbisch^{1,2,4}

¹ Museum für Naturkunde, Leibniz-Institut für Evolutions- und Biodiversitätsforschung, Berlin, Germany

² Institut für Biologie, Humboldt-Universität zu Berlin, Berlin, Germany

³ North Carolina Museum of Natural Sciences, Raleigh, NC, USA

⁴ Evolutionary Studies Institute, University of the Witwatersrand, Johannesburg, South Africa

ABSTRACT

The cynodont fauna of the *Trirachodon-Kannemeyeria* Subzone of the Middle Triassic *Cynognathus* Assemblage Zone (AZ) is almost exclusively represented by taxa belonging to the clade Eucynodontia. However, there is one basal (non-eucynodont) cynodont known to have survived into this assemblage: the enigmatic *Bolotridon frerensis*. BSPG 1934-VIII-7 represents by far the most extensive specimen of *B. frerensis*, consisting of a partial skull with occluded lower jaw. The specimen was initially described by *Broili & Schröder (1934)*, but their description was limited to surface details of the skull and the dental morphology. Here, by using a computed tomographic (CT) reconstruction, we redescribe this specimen, providing novel information on its palatal and internal anatomy. New endocranial characters recognized for this taxon include ridges in the nasal cavity indicating the presence of cartilaginous respiratory turbinates. New data obtained from the CT scan were incorporated into the most recently published data matrix of early non-mammalian cynodonts to test the previously unstable phylogenetic position of *Bolotridon*. Our phylogenetic analyses recovered *Bolotridon* as the sister-taxon of Eucynodontia, a more crownward position than previously hypothesized.

Subjects Evolutionary Studies, Paleontology, Taxonomy, Zoology

Keywords Therapsida, Computed tomography, Endocranial anatomy, Phylogeny

INTRODUCTION

Cynodontia is one of the six major therapsid subclades and was the last to diversify, first appearing in the fossil record in the late Permian but not showing substantial species richness until the Middle Triassic, when it became the most diverse and abundant synapsid group (*Hopson & Kitching, 1972; Kemp, 2005; Abdala & Ribeiro, 2010; Angielczyk & Kammerer, 2018; Lukic-Walther et al., 2019*). In the form of their mammalian descendants, cynodonts remained the most successful synapsid lineage throughout the Mesozoic and onwards to the present day. By contrast, early in their history cynodonts are a minor component of terrestrial ecosystems, and with a few notable exceptions (e.g., *Galesaurus*,

Submitted 24 March 2021

Accepted 10 May 2021

Published 16 June 2021

Corresponding author

Luisa C. Pusch,
luisa.pusch@mfn.berlin

Academic editor

Brandon Hedrick

Additional Information and
Declarations can be found on
page 23

DOI 10.7717/peerj.11542

© Copyright
2021 Pusch et al.

Distributed under
Creative Commons CC-BY 4.0

OPEN ACCESS

Thrinaxodon) are rare and poorly known from late Permian and earliest Triassic faunas. However, recent work has improved our knowledge of early cynodont diversity. [Abdala et al. \(2019\)](#) described a new, surprisingly large cynodont taxon (*Vetusodon elikhulu*) from the late Permian (Lopingian) of the Karoo Basin in South Africa, and [Huttenlocker & Sidor \(2020\)](#) described another new taxon (*Nshimbodon muchingaensis*) from the upper Permian Madumabisa Mudstone Formation of Zambia. In addition to *Vetusodon*, five further Permian cynodont taxa are currently recognized from the Karoo Basin: *Charassognathus gracilis* and *Abdalodon diastematicus* (the oldest known cynodonts, currently known from a single skull each from the upper *Endothiodon* Assemblage Zone (AZ)), *Procynosuchus* (a broadly-distributed taxon with additional records from elsewhere in Africa and in Europe), and *Cynosaurus suppostus* and *Nanictosaurus kitchingi*. The latter two species may represent early representatives of primarily Triassic lineages, suggesting that the cynodont radiation had begun prior to the end-Permian mass extinction ([Broom, 1937](#); [Kemp, 1979](#); [Van Heerden & Rubidge, 1990](#); [Abdala & Allinson, 2005](#); [Botha, Abdala & Smith, 2007](#); [Kammerer, 2016](#); [Van den Brandt & Abdala, 2018](#); [Abdala et al., 2019](#); [Viglietti, 2020](#)).

None of the late Permian genera are known to have survived the end-Permian mass extinction, but at least two lineages (Galesauridae and Thrinaxodontidae) seem to have crossed the Permo-Triassic boundary, and were fairly abundant in the Lower Triassic *Lystrosaurus declivis* AZ of the Karoo Basin in South Africa ([Botha & Smith, 2020](#)). Galesaurids are represented in the Triassic by the taxa *Galesaurus* and *Progalesaurus* (e.g., [Sidor & Smith, 2004](#); [Pusch, Kammerer & Fröbisch, 2019](#)), whereas Thrinaxodontidae is represented by the extremely common and extensively studied taxon *Thrinaxodon* (e.g., [Fourie, 1974](#); [Rowe, Carlson & Bottorff, 1995](#); [Abdala, Jasinowski & Fernandez, 2013](#); [Jasinowski, Abdala & Fernandez, 2015](#)). A rarer representative of early cynodonts in the *Lystrosaurus declivis* AZ is the unusually broad-skulled genus *Platycraniellus* ([Abdala, 2007](#)). By the Middle Triassic, these taxa had disappeared, with later Triassic cynodonts consisting almost exclusively of members of the diverse clade Eucynodontia. At least seven genera of eucynodonts are recorded in the Middle Triassic *Cynognathus* AZ (and additional, undescribed taxa are also probably present; see [Hendrickx et al. \(2020\)](#)): the cynognathians *Cynognathus*, *Diademodon*, *Langbergia*, *Cricodon*, and *Trirachodon*, the probainognathian *Lumkuia*, and the phylogenetically uncertain taxon *Cistecynodon* ([Brink & Kitching, 1953](#); [Hopson & Kitching, 2001](#); [Abdala & Giannini, 2002](#); [Sidor & Smith, 2004](#); [Abdala, Hancox & Neveling, 2005](#); [Abdala & Ribeiro, 2010](#)). Most of these genera (all but *Langbergia* and *Cricodon*) are known from the most extensively-exposed and best-studied portion of the *Cynognathus* AZ, the *Trirachodon*-*Kannemeyeria* Subzone ([Hancox, Neveling & Rubidge, 2020](#)).

One additional cynodont taxon is currently recognized from the *Trirachodon*-*Kannemeyeria* Subzone, the enigmatic *Bolotridon frerensis*. Preliminary studies have suggested that *Bolotridon* (= *Tribolodon*; see [Coad \(1977\)](#)) is the only basal (i.e., non-eucynodont) cynodont to survive into the Middle Triassic ([Sidor & Smith, 2004](#); [Abdala, Hancox & Neveling, 2005](#); [Abdala & Ribeiro, 2010](#)). However, the rarity and incompleteness of the known material of this taxon have made it difficult to resolve its

phylogenetic position, which has been tested computationally in only one analysis ([Sidor & Smith, 2004](#)). [Hopson & Kitching \(1972\)](#) regarded *Bolotridon* as a member of the family Galesauridae, albeit in a pre-cladistic sense containing all non-eucynodont epicynodonts, rather than an indication of any particular relationship to *Galesaurus*. [Battail \(1991\)](#) included *Bolotridon* in the family Thrinaxodontidae based on the possible presence of a complete osseous palate. However, the presence of a complete secondary palate has never been confirmed for *Bolotridon*. The earliest definite presence of this mammal-like feature in cynodonts occurs in thrinaxodontids, and this character is then retained in all crownward taxa ([Fourie, 1974](#); [Van Heerden & Rubidge, 1990](#); [Hopson, 1991](#); [Crompton, Musinsky & Owerkowicz, 2015](#); [Crompton et al., 2017](#)). An exception to its universal retention has recently been suggested for the Permian *Vetusodon*, which has an incomplete secondary palate, but was recovered crownward of *Thrinaxodon* in the initial analysis of [Abdala et al. \(2019\)](#). However, the most recent phylogeny by [Huttenlocker & Sidor \(2020\)](#) supports a more basal position for *Vetusodon*, placing it with *Cynosaurus* near the base of Epicynodontia (outside of the origin of the complete secondary palate).

The holotype of *Bolotridon frerensis* is a partial left dentary (NHMUK PV R2583), which was described by [Seeley \(1894, 1895\)](#) and collected at the historic *Cynognathus* AZ locality of Lady Frere Commonage (Cacadu, Chris Hani District Municipality, Eastern Cape Province) in South Africa. A right femur and left tibia (NHMUK PV R2584) were found together with the holotype while removing matrix from a skull of “*Gomphognathus*” (= *Diademodon*) ([Seeley, 1895](#)) and have been referred to *B. frerensis* as well, but the association of these elements with the holotype jaw is questionable. The majority of other referred specimens from the type locality also only represent isolated dentary or maxillary elements (BSPG 1934-VIII-8, 9, 501, 502, 503, 504, and 505) and do not provide further information on the broader anatomy of this taxon. The sole exception to this is the specimen BSPG 1934-VIII-7, which is by far the most complete known specimen of *B. frerensis* and consists of a partial skull with occluded lower jaw ([Figs. 1–3](#)). [Broili & Schröder \(1934\)](#) provided an initial description of BSPG 1934-VIII-7, but their description was limited to surface details and focused on the dental morphology of this and other referred specimens. The tight occlusion of the upper and lower jaws also prevented the authors from exposing the palatal region without damaging the skull through overpreparation. Accordingly, the morphology of the palate remains largely unknown.

Here, we present a redescription of *Bolotridon frerensis* based on computed tomographic (CT) reconstruction of BSPG 1934-VIII-7. This provides new insights into the previously-obscured palatal region and novel information on endocranial characters in this taxon. Although the palate is damaged in BSPG 1934-VIII-7, our redescription provides substantial new data on its anatomy allowing incorporation into the most recent published data matrix of basal cynodonts ([Huttenlocker & Sidor, 2020](#)). This new information is used to test the currently unstable phylogenetic placement of *Bolotridon* ([Hopson & Kitching, 1972](#); [Battail, 1991](#); [Sidor & Smith, 2004](#)). We also discuss the faunal composition of the *Cynognathus* AZ, with a special focus on Lady Frere Commonage, which yields seemingly unusual faunal elements not recorded in other exposures of this assemblage zone.

MATERIALS & METHODS

Specimen

The specimen of *Bolotridon frerensis* described herein (BSPG 1934-VIII-7; [Figs. 1–9](#)) is part of the collection of the Bayerische Staatssammlung für Paläontologie und Geologie in Munich. The block containing the fossil remains of this and most other referred specimens of *B. frerensis* (BSPG 1934-VIII-8, 9, 501, 502, 503, 504, and 505) was collected in the Burgersdorp Formation, in exposures representing the *Trirachodon-Kannemeyeria* Subzone of the Middle Triassic *Cynognathus* AZ. It was discovered by G. Grossarth at Lady Frere Commonage in 1931, as part of a research trip by the Bayerische Akademie der Wissenschaften. The specimens were later prepared by the technician G. Kochner of the same institution ([Broili & Schröder, 1934](#)). The skull of BSPG 1934-VIII-7 is laterally compressed and cracked, but the dentition and many of the individual cranial elements are in good condition. The total length of the specimen is 8.1 cm and its maximum width is ~3.7 cm.

Computed tomography data

BSPG 1934-VIII-7 was CT scanned in the CT-Laboratory of the Museum für Naturkunde Berlin using an YXLON FF35 X-ray CT scanner with a voxel size of 0.0463 mm, a voltage of 115 kV and a current of 220 μ A. The visualization of the slices, virtual 3D rendering, and segmentation of selected structures were performed using VGStudio Max 3.3 (Volume Graphics GmbH, Heidelberg, Germany) in the 3D Visualization Laboratory at the Museum für Naturkunde Berlin.

Phylogenetic analyses

BSPG 1934-VIII-7 was coded into the dataset of the most recent phylogenetic analysis of early non-mammalian cynodonts ([Huttenlocker & Sidor, 2020](#)) to assess its relationships. The matrix of [Huttenlocker & Sidor \(2020\)](#) was largely modified from those of [Abdala \(2007\)](#) and [Kammerer \(2016\)](#) and contains a few newly adapted characters from other sources. We reduced the number of characters in their matrix from 111 to 110, because one character was present twice (character 27 = 64; we deleted the repeated character 64). The data matrix further comprises 26 therapsid taxa: two gorgonopsians (*Aelurognathus* and *Cyonosaurus*) used as outgroups, eight therocephalians, and 16 cynodonts including the newly added *Bolotridon*. A parsimony analysis was performed in PAUP 4.0a (build 168) ([Swofford, 2003](#)), with minimum branch lengths of zero set to collapse. For the analysis, a heuristic search with tree-bisection-reconnection (TBR) branch-swapping was performed, with multistate characters unordered. A bootstrap analysis was conducted based on 1,000 replicates to assess clade support. Additionally, a Bayesian analysis was performed in MrBayes v. 3.2.7 ([Ronquist & Huelsenbeck, 2003](#)) using the Markov model ([Lewis, 2001](#)) with a gamma distributed rate parameter. The Markov chain Monte Carlo analysis ran for one million generations (run time 15.11 min) until the standard deviation of split frequencies fell below 0.01. The results of both analyses are included into the updated character list ([Data S1](#)) and the updated data matrix can be found in [Data S2](#) and [S3](#).

RESULTS

General preservation

The skull of BSPG 1934-VIII-7 is missing the septomaxillae, temporal region, and occiput. It is laterally compressed, with the right half of the skull having been shifted somewhat posteriorly and ventrally and the left half somewhat anteriorly and dorsally (Figs. 1–3). A small fragment of bone is preserved lateral to the coronoid process of the right dentary and posterior to the jugal, which might pertain to the squamosal (Figs. 1, 2, 4) (this element is otherwise not preserved in this specimen). The palate of BSPG 1934-VIII-7 was strongly affected by lateral compression, and resolution of the palate in the CT-scan is not ideal, but the scan still provides substantial information about the morphology of this region that is not visible externally (Figs. 5, 7). The lower jaw of BSPG 1934-VIII-7 consists of the dentaries, right splenial, anterior portion of the left angular, and prearticulars, with the right prearticular being more complete. The left prearticular is preserved only as a small fragment. The left splenial, right angular, and both surangulars, coronoids, and articulars are missing in this specimen (Figs. 1–4, 8).

Snout

The premaxilla is a small bone forming the anteriormost margin of the snout and the anteromedial and ventral margins of the external naris. Its prenasal (intranarial) process, which is slightly damaged ventrally, extends dorsally to contact the nasals (Figs. 1–4). The facial portion of the premaxilla is posteriorly overlain by the maxilla up to the level of the fourth incisor (Figs. 2, 3). Each premaxilla bears four conical, slightly recurved incisors, which appear unusually long in *Bolotridon* compared to other basal cynodonts (although their apparent length could be an artifact of slipping out of their sockets post mortem). The left incisor row has been slightly shifted forward, with the result that the left I4 is positioned around the same level as the right I3, and the right I1 and left I1, I2 and I3 are very close together. The fourth incisor on both sides is considerably smaller than the preceding three teeth. The right I4 has partially fallen out of its socket and is displaced posteroventrally. Posteromedially, the premaxilla forms a broad plate underlying the anterior portion of the vomer. At the posterolateral margin of this plate, the premaxilla is separated from the maxilla by an oval paracanine fossa accommodating the crown of the lower canine. This fossa is positioned anteromedial to the canine, as is usual for basal cynodonts. Lateral to the paracanine fossa, a short diastema is present between I4 and the upper canine (Figs. 2, 3, 4, 7B).

The dorsal roof of the snout and nasal cavity is formed by elongate nasal bones. The nasals are transversely narrow at their anterior edge, and narrow further (appearing ‘pinched’ in dorsal view) at mid-length where they are overlapped by the dorsal edges of the maxillae before broadening posteriorly. The nasals contact the frontals posteriorly and the lacrimals and prefrontals posterolaterally, around the level of the anterior orbital margin (Figs. 1, 2, 3, 6). In internal view, the ventral margin of the nasal bone projects deeply into the nasal cavity and is slightly overlapped by the anterior and dorsal portion of the lacrimal posteriorly (Figs. 4, 5B). The underside of the nasals is generally concave, but

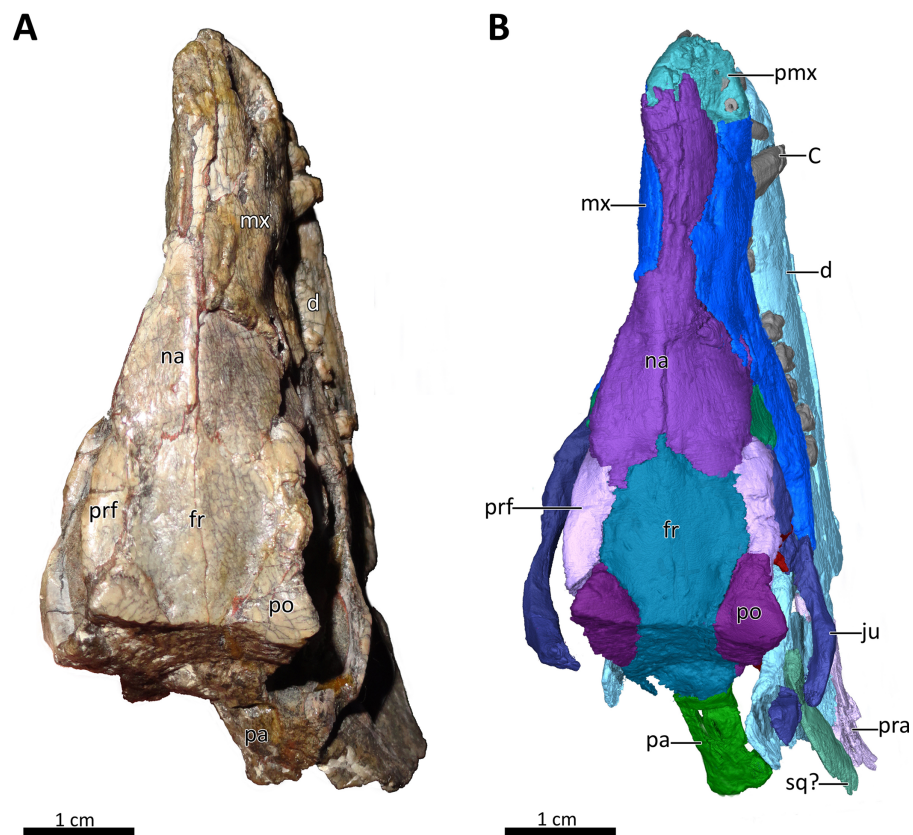


Figure 1 BSPG 1934-VIII-7 in dorsal view. (A) Photograph and (B) 3D reconstruction of the specimen. Abbreviations: C, upper canine; d, dentary; fr, frontal; ju, jugal; mx, maxilla; na, nasal; pa, parietal; pmx, premaxilla; po, postorbital; pra, prearticular; prf, prefrontal; sq?, squamosal?. Photograph in (A) by Christian F. Kammerer. Image of the 3D reconstructed skull in (B) by Luisa C. Pusch.

Full-size [DOI: 10.7717/peerj.11542/fig-1](https://doi.org/10.7717/peerj.11542/fig-1)

becomes flatter in the region where they contact the lacrimals. It is characterized by a series of ridges extending anteriorly from the interorbital region along the ventral surface of the frontals and continuing onto the nasals. These ridges consist of a median ridge along the midline suture, which weakens anteriorly, and a pair of lateral ridges running parallel to the median ridge (Figs. 5B, 6). Similar ridges are known from a number of therapsids and have been interpreted as attachment points for cartilaginous nasal turbinals, with the median ridge possibly supporting the dorsal edge of a cartilaginous nasal septum (e.g., Kemp, 1979; Hillenius, 1994; Sigurdson, 2006; Crompton, Musinsky & Owerkowicz, 2015; Crompton et al., 2017; Bendel et al., 2018; Pusch, Kammerer & Fröbisch, 2019; Pusch et al., 2020; Huttenlocker & Sidor, 2020).

The maxilla is a large bone that extends over most of the lateral surface of the snout and forms much of the sidewall of the nasal cavity and the secondary palate (Figs. 1–4, 7). Medially, the two maxillae contact one another on the ventral surface of the snout. Unfortunately, because of strong lateral compression, it is uncertain whether the maxillae naturally contacted one another to form a complete secondary palate. The maxillae are clearly distorted to some degree, as both palatal processes have been shifted against each

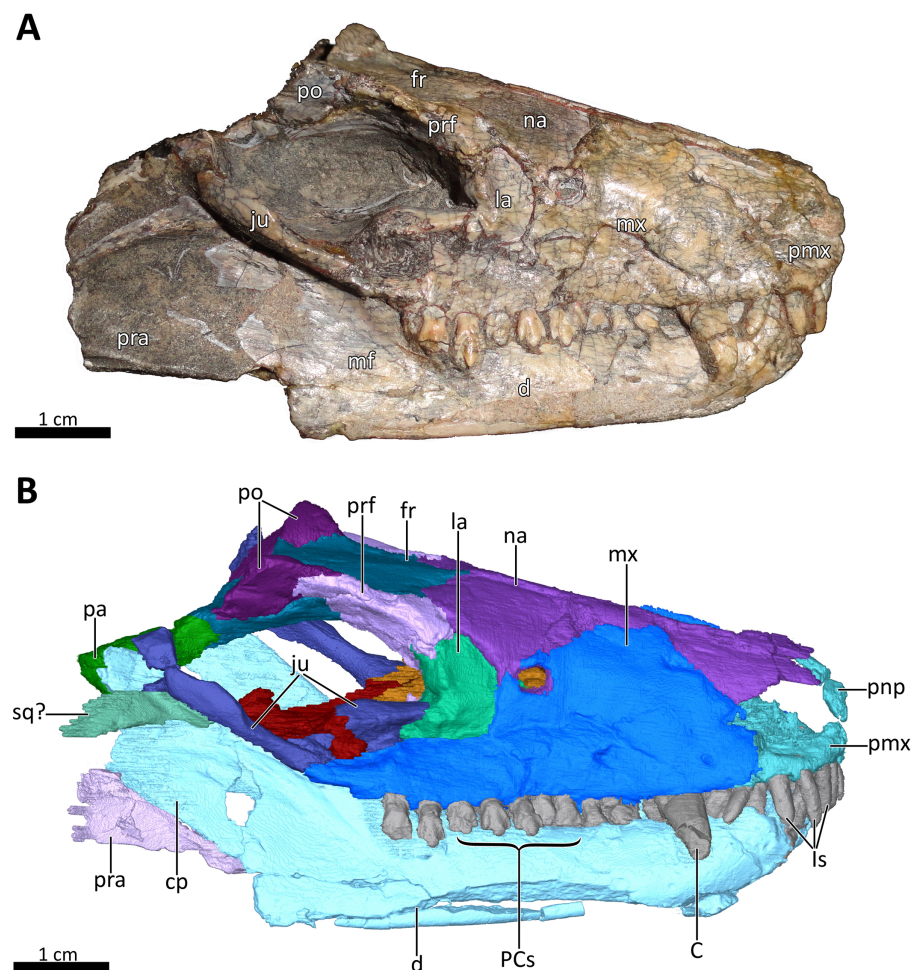


Figure 2 BSPG 1934-VIII-7 in right lateral view. (A) Photograph and (B) 3D reconstruction of the specimen. *Abbreviations:* C, upper canine; cp, coronoid process; d, dentary; fr, frontal; Is, upper incisors; ju, jugal; la, lacrimal; mf, masseteric fossa; mx, maxilla; na, nasal; pa, parietal; PCs, upper postcanines; pmx, premaxilla; pnp, prenasal process of the premaxilla; po, postorbital; pra, prearticular; prf, prefrontal; sq?, squamosal?. Photograph in (A) by Christian F. Kammerer. Image of the 3D reconstructed skull in (B) by Luisa C. Pusch. [Full-size !\[\]\(fd7fe780e8fd8eece60268c87d0c3e04_img.jpg\) DOI: 10.7717/peerj.11542/fig-2](https://doi.org/10.7717/peerj.11542/fig-2)

other, with the right palatal process overlapping the left one (Fig. 7B). A similar case of deformation-induced contact of the medial projections of the maxillae was recently described for the Early Triassic cynodont *Galesaurus* (Pusch, Kammerer & Fröbisch, 2019) (undistorted *Galesaurus* skulls indicate that this taxon did not have a complete secondary palate). Despite their damage, based on the proportions of the maxillary projections in *Bolotridon*, the secondary palate of this taxon must have been at least as extensive as in *Galesaurus* (i.e., more expansive than in Permian cynodonts such as *Procynosuchus*, *Dvinia*, *Abdalodon* and *Vetusodon*, in which the medial processes are transversely shorter; Tatarinov, 1968; Kemp, 1979; Hopson & Kitching, 2001; Ivakhnenko, 2013; Kammerer, 2016; Abdala et al., 2019).

Both the external and internal surfaces of the maxillae are generally smooth, although the external surfaces of both maxillae are marked by some slight cracks (Figs. 2, 3, 4).

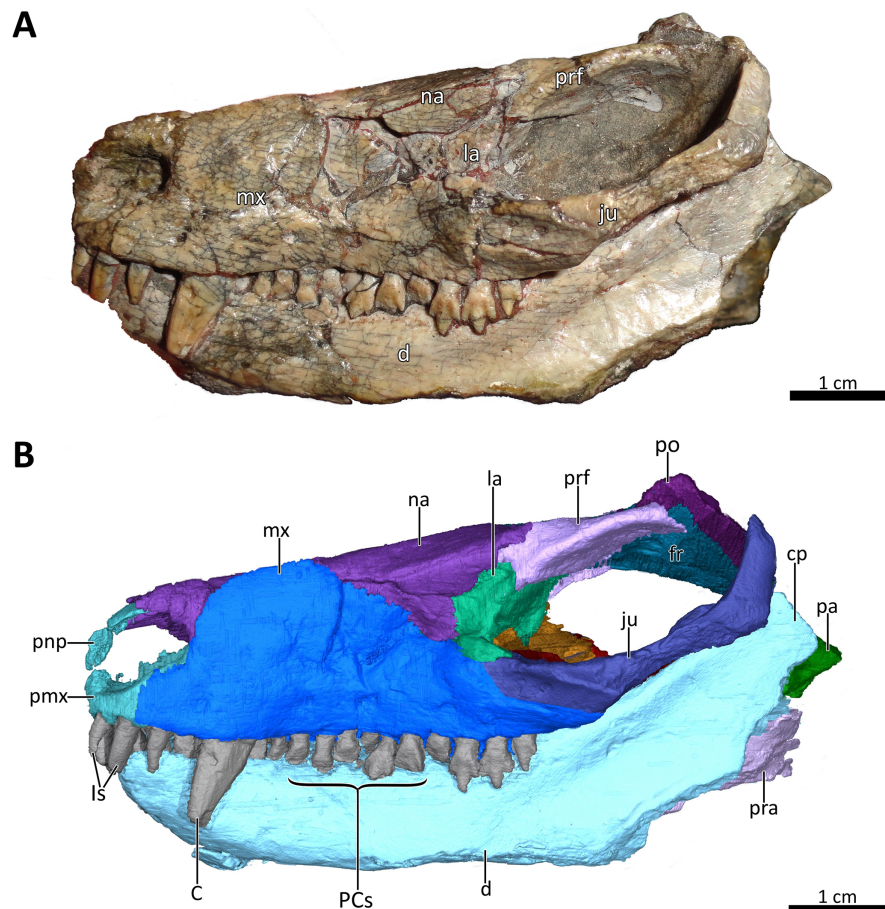


Figure 3 BSPG 1934-VIII-7 in left lateral view. (A) Photograph and (B) 3D reconstruction of the specimen. *Abbreviations:* C, upper canine; cp, coronoid process; d, dentary; fr, frontal; Is, upper incisors; ju, jugal; la, lacrimal; mx, maxilla; na, nasal; pa, parietal; PCs, upper postcanines; pmx, premaxilla; pnp, prenasal process of the premaxilla; po, postorbital; pra, prearticular; prf, prefrontal. Photograph in (A) by Christian F. Kammerer. Image of the 3D reconstructed skull in (B) by Luisa C. Pusch.

Full-size  DOI: [10.7717/peerj.11542/fig-3](https://doi.org/10.7717/peerj.11542/fig-3)

The internal surface of the maxilla is dorsally strongly overlapped by the ventral margin of the nasals and anteriorly it is covered by the palatal process of the premaxilla. Posteriorly, it is overlapped by the anterior margins of the lacrimal and jugal, and also by the dorsolateral portions of the damaged and displaced palatine (Figs. 4, 5, 7A). Three large foramina perforate the external surface of the maxilla above the tooth row, marking the openings of rami from the maxillary canal. Unfortunately, we were unable to resolve the course of the maxillary canal in the CT-scan, as it was damaged due to the strong compression of the snout.

A total of nine right and eleven left upper postcanines are present in BSPG 1934-VIII-7 (Figs. 2, 3, 7B). The number of upper postcanines slightly differs from what was described by *Broili & Schröder (1934)*, who originally counted ten postcanines in the left maxilla. The discrepancy is likely due to the tight occlusion of upper and lower jaws, making it difficult to see the actual number of the teeth without CT data. The postcanines increase in

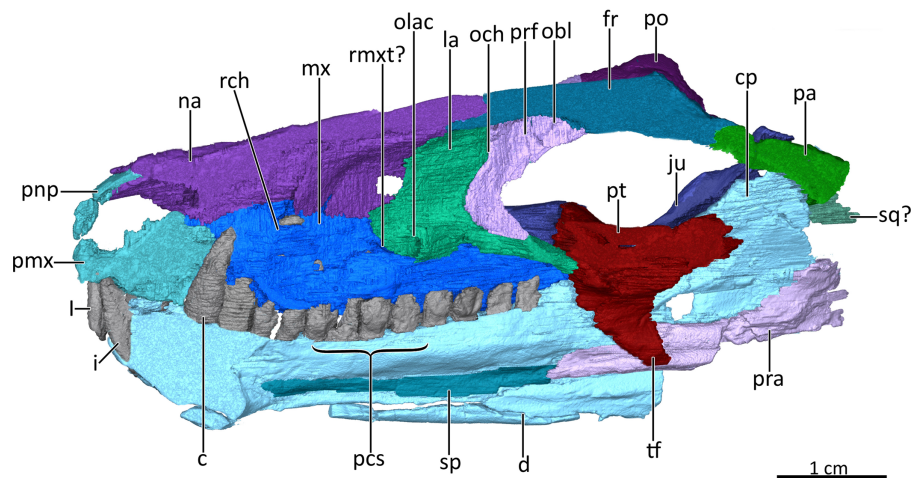


Figure 4 Mid sagittal section through the reconstructed skull and lower jaw of BSPG 1934-VIII-7, with the vomer and palatine digitally removed to show the internal morphology. *Abbreviations:* c, lower canine; cp, coronoid process; d, dentary; fr, frontal; I, upper incisor; i, lower incisor; ju, jugal; la, lacrimal; mx, maxilla; na, nasal; obl, olfactory bulb location; och, olfactory chamber; olac, opening of lacrimal canal; pa, parietal; pcs, lower postcanines; pmx, premaxilla; pnp, prenasal process of the premaxilla; po, postorbital; pra, prearticular; prf, prefrontal; pt, pterygoid; rch, respiratory chamber; rmxt?, ridge for cartilaginous maxilloturbinals?; sp, splenial; sq?, squamosal?, tf, transverse flange of the pterygoid. Image by Luisa C. Pusch

Full-size [DOI: 10.7717/peerj.11542/fig-4](https://doi.org/10.7717/peerj.11542/fig-4)

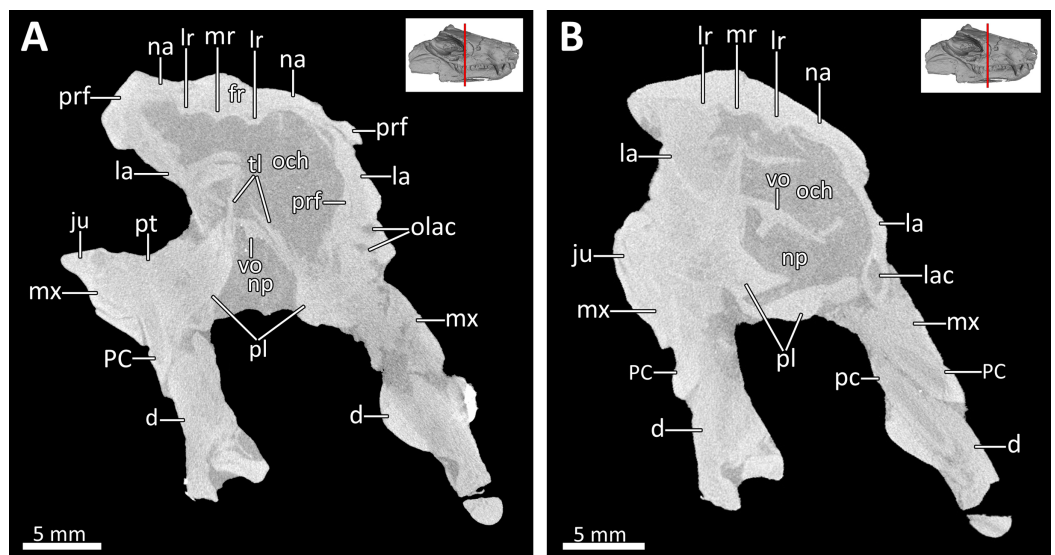


Figure 5 Transverse CT sections through the olfactory chamber (A, B) of BSPG 1934-VIII-7. *Abbreviations:* d, dentary; fr, frontal; ju, jugal; la, lacrimal; lac, lacrimal canal; lr, lateral ridge; mr, median ridge; mx, maxilla; na, nasal; np, nasopharyngeal passage; och, olfactory chamber; olac, opening of lacrimal canal; PC, upper postcanine; pc, lower postcanine; pl, palatine; prf, prefrontal; pt, pterygoid; tl, transverse lamina; vo, vomer. CT images in (A) and (B) by Luisa C. Pusch.

Full-size [DOI: 10.7717/peerj.11542/fig-5](https://doi.org/10.7717/peerj.11542/fig-5)

size from the first to the penultimate tooth. The last postcanine is noticeably smaller than the penultimate tooth in the left maxilla. On the right side the last postcanine is damaged, but appears comparable in size to its predecessor, suggesting that the small size

of the left last postcanine could be a result of its recent eruption at the time of death. However, several postcanines have damaged crowns, with only the left PC6, PC9, PC10, and PC11 and the right PC5, PC6, and PC8 being completely preserved, showing the tricuspid morphology described by *Broili & Schröder (1934)*. Notable is the morphology of the intact left PC6 and right PC5 and PC6, which appear to naturally have a shorter main cusp than the more posterior teeth, in which the main cusp is more pronounced. This is most clearly visible in the left PC9, PC10, and PC11 (Figs. 2, 3). The presence of two separated lingual cingular cusps cannot be observed for both upper and lower postcanines in BSPG 1934-VIII-7 due to damage, but have been described in other referred specimens of *B. frerensis* with better preserved teeth (*Broili & Schröder, 1934*). There is a short diastema present between the upper canine and the anteriormost upper postcanine, with the left canine being relatively well preserved, whereas in the right canine the crown is more damaged. Serrations are absent on all teeth, and distinct carinae are not present on the canines (Figs. 2, 3, 7B, 8).

The anterior margin of the orbit is formed by the lacrimal, which contacts the prefrontal dorsally, the nasal anterodorsally, the maxilla anteriorly and the anterior part of the jugal posteroventrally (Figs. 2, 3). The medial surface of the lacrimal is posteriorly overlapped by the anterior and ventral margins of the prefrontal. Anteriorly, it covers part of the posterior portion of the maxilla. Its medial surface contacts the palatine, although the extent of this contact has been exaggerated due to compression (Fig. 5B). On the floor of the orbit, the posteroventral extension of the lacrimal also contacts the pterygoid and covers the anterior part of the jugal. The lacrimal is perforated posteriorly by two small foramina, through which the nasolacrimal canal originates in the anterior edge of the orbit. The canal runs anteriorly through a ridge on the medial surface of the lacrimal and opens at the level of the sixth lower postcanine above a small maxillary antrum, which was only weakly visible in the scan (Figs. 4, 5). A short ridge appears to extend slightly forward beyond this opening (Fig. 4). In the 3D reconstruction it resembles the structure described for *Galesaurus* (*Pusch, Kammerer & Fröbisch, 2019*) and *Thrinaxodon* (*Crompton, 2013*). However, we cannot exclude the possibility that this is just a crack caused by damage and compression of the maxilla in that area. Clear evidence of ridges extending forward beyond the opening of the lacrimal canal have so far been provided for only a few non-mammalian cynodonts, with their earliest appearance in *Galesaurus* and *Thrinaxodon*, and have been interpreted as forming the base for cartilaginous maxilloturbinals (*Fourie, 1974; Hillenius, 1994; Crompton, 2013; Crompton, Musinsky & Owerkowicz, 2015; Crompton et al., 2017; Pusch, Kammerer & Fröbisch, 2019*).

The prefrontal contributes to the anterodorsal edge and also partly to the medial wall of the orbit. Its anterodorsal portion contacts the nasal anteriorly and the lacrimal ventrally, and its posterodorsal portion contacts the postorbital posteriorly (Figs. 1, 2, 3, 6). The suture between the prefrontal and nasal is relatively short in BSPG 1934-VIII-7, related to the small size and slender shape of the prefrontal. The contact between the nasal and lacrimal is accordingly somewhat longer than what is usually observed in basal cynodonts, in which the prefrontal tends to be a larger bone occupying more of this region (e.g., *Fourie, 1974; Kemp, 1979; Sidor & Smith, 2004; Abdala, 2007; Botha, Abdala & Smith,*

2007; Kammerer, 2016; Van den Brandt & Abdala, 2018; Abdala et al., 2019; Pusch, Kammerer & Fröbisch, 2019). The dorsal margin of the prefrontal is curved and projects inwards to overlap the anterolateral process of the lateral flange of the frontal. In internal view, its anterior margin also slightly overlies the lacrimal along its posterior and posteroventral margins (Figs. 1–4, 5A, 6).

The incomplete jugals make up the posterolateral floor of the orbit and the ventral portion of the zygomatic arch. They contact the maxilla anteriorly, the lacrimal anterodorsally and the anterolateral portion of the pterygoid medially. The better preserved left jugal also slightly contacts the posterolateral tip of the palatine. A contact of the jugal with the palatine seems to be naturally present, as has also been described for *Galesaurus* (Pusch, Kammerer & Fröbisch, 2019). The missing contact between these bones on the right side is likely an artifact of deformation caused by shifting of the skull halves. In internal view, the jugal is anteriorly overlapped by the posteroventral margin of the lacrimal, which is in turn overlapped by the prefrontal. The jugal forms the ventral portion of the postorbital bar, in the form of a dorsally-directed ‘spike’ that would have contacted the postorbital bone (preserved on the left side only). The posterior preserved tip of the right jugal contacts the fragmented piece of bone that might belong to the squamosal (Figs. 1–4, 7).

Skull roof

The frontals are anteroposteriorly elongate bones extending between the nasals anteriorly and the parietals (of which only a fragment is preserved that does not provide much information on the morphology of the bone) posteriorly. Anterolaterally, the frontal’s lateral flange is overlapped by the curved dorsal margin of the prefrontal, and posterolaterally it contacts the dorsal part of the postorbital (Figs. 1–4, 5A). A deep, elongate depression on the ventral surface of the frontals, which is divided by a faint median ridge into left and right compartments, marks the location for the olfactory bulbs of the brain. The lateral and partial anterior limit of the olfactory bulbs is bounded by two ridges, which weaken anteriorly until they meet a pronounced ridge at the midline suture of the frontals marking the hindmost part of the nasal cavity (Figs. 4, 5A, 6). Similar ridges bounding the olfactory bulbs have been described for the basal cynodonts *Procynosuchus* (Kemp, 1979) and *Galesaurus* (Pusch, Kammerer & Fröbisch, 2019), as well as the probainognathian *Chiniquodon* (Kemp, 2009). The posterior limit of the olfactory bulbs is likely indicated by the gradual transition from slight concavity to convexity of the ventral surface of the frontals at the level of the postorbital bar (Figs. 4, 6). The pronounced ridge originating at the midline suture of the frontals just anterior to the depression housing the olfactory bulbs of the brain also marks the posterior limit of the cartilaginous nasal septum, which was likely attached to the median ridge (Crompton, Musinsky & Owerkiewicz, 2015; Crompton et al., 2017).

The postorbitals are badly damaged, with only their anterior portion being preserved. The postorbital contributes to the dorsal margin of the orbit by contacting the posterior portion of the prefrontal anterodorsally and the posterior portion of the frontals

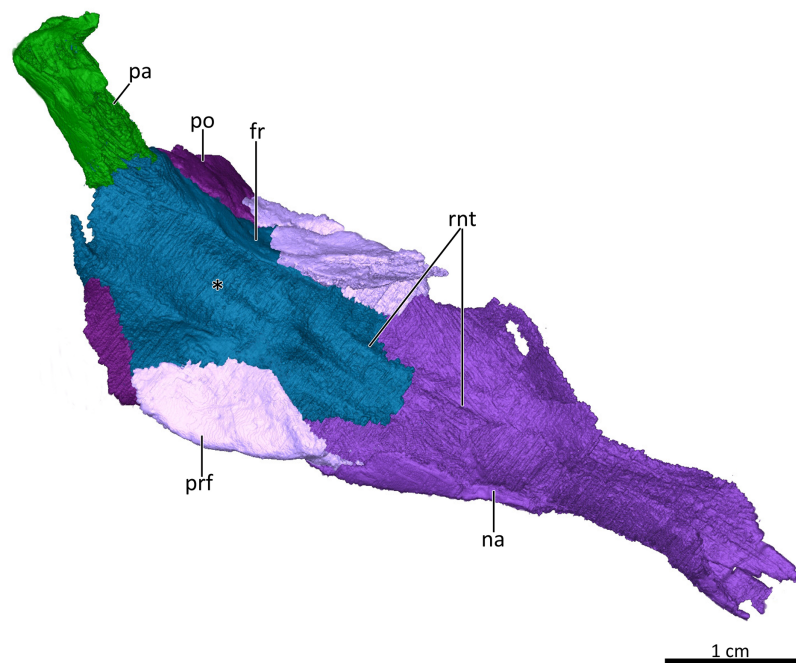


Figure 6 3D reconstruction of the skull roof in ventrolateral view. Asterisk marks the location of the olfactory bulbs of the brain on the ventral surface of the frontals. *Abbreviations:* fr, frontal; na, nasal; pa, parietal; po, postorbital; prf, prefrontal; rnt, ridge for cartilaginous nasal turbinals. Image by Luisa C. Pusch. [Full-size !\[\]\(a6fe094a331555a6fd67d72f7f1bf63e_img.jpg\) DOI: 10.7717/peerj.11542/fig-6](https://doi.org/10.7717/peerj.11542/fig-6)

dorsolaterally. It also would have formed the posterodorsal portion of the postorbital bar, though its descending ramus contacting the jugal is not preserved (Figs. 1, 2, 3, 6).

Palate

The morphology of the strongly compressed and displaced unpaired vomer is difficult to resolve in the scan of BSPG 1934-VIII-7. It is an elongated strip of bone dividing the nasopharyngeal passage at the midline, which appears to be very narrow as a result of lateral compression of the skull halves (Figs. 5, 7). The anterior portion of the vomer, which overlies the palatal process of the premaxilla (Fig. 7A), is usually characterized by having a grooved dorsal surface housing the vomeronasal organ in therapsids (e.g., *Hillenius, 2000; Crompton et al., 2017; Kammerer, 2017; Bendel et al., 2018; Pusch, Kammerer & Fröbisch, 2019; Pusch et al., 2020*). However, in BSPG 1934-VIII-7 the anterior portion of the vomer is clearly damaged, and the housing for the vomeronasal organ is not evident (Fig. 7A). The posterior portion of the vomer has two lateral ‘wings’, which are not in their natural positions, with the left wing also being bent ventrally due to damage. These wings are wedged posteriorly between the medially directed plates of the palatines, together forming a transverse lamina, which forms the posterior border of the long primary choanae that extend the length of the vomer and open into the nasopharyngeal passage (Figs. 5, 7A), as has also been described for *Galesaurus* (*Pusch, Kammerer & Fröbisch, 2019*), *Thrinaxodon* (*Crompton, 2013*) and the more crownward eucynodonts *Massetognathus* and *Probainognathus* (*Crompton, Musinsky & Owerkowicz,*

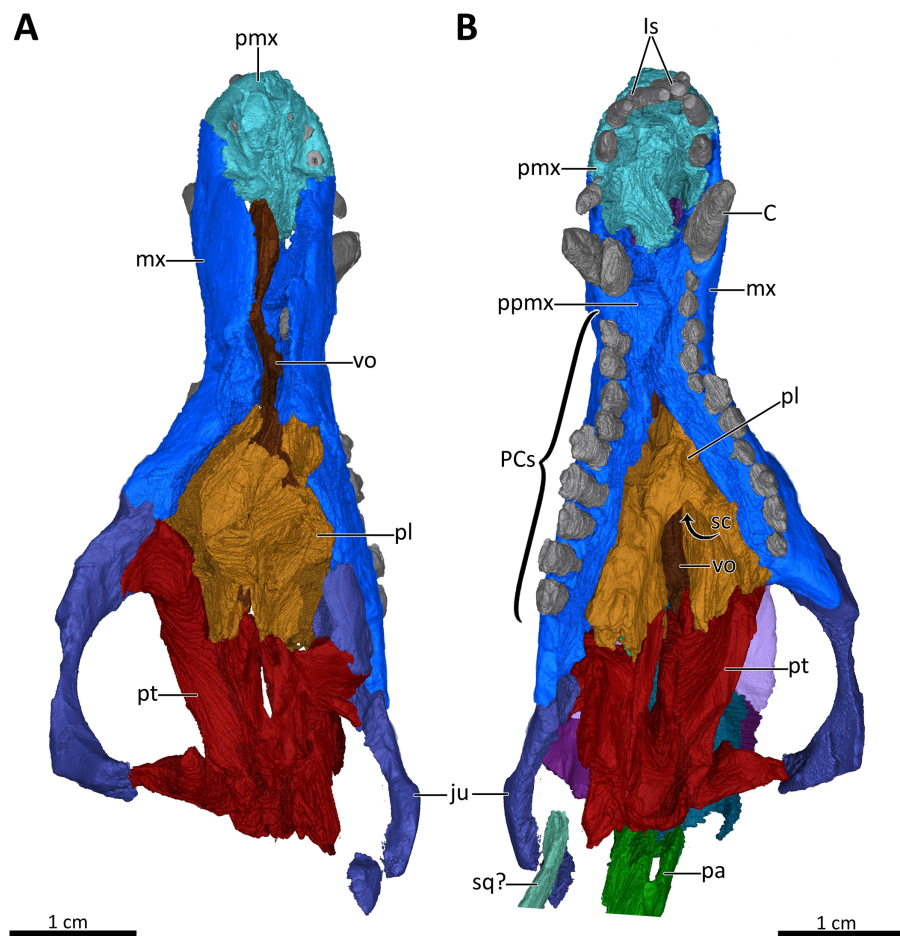


Figure 7 3D reconstruction of the snout of BSPG 1934-VIII-7. (A) Snout in dorsal aspect with the nasals, lacrimals, prefrontals, postorbitals, frontals, parietal and squamosal digitally removed to expose its internal structure. (B) Ventral view of the palate. *Abbreviations:* C, upper canine; ls, upper incisors; ju, jugal; mx, maxilla; pa, parietal; PCs, upper postcanines; pl, palatine; pmx, premaxilla; ppmx, palatal process of the maxilla; pt, pterygoid; sc, secondary choana; sq?, squamosal?; vo, vomer. Images in (A) and (B) by Luisa C. Pusch. [Full-size !\[\]\(f5a508cc6d05e5d06b117ced927b1acd_img.jpg\) DOI: 10.7717/peerj.11542/fig-7](https://doi.org/10.7717/peerj.11542/fig-7)

2015; Crompton et al., 2017). As has been suggested by Hillenius (1994), Crompton et al. (2017), and Pusch, Kammerer & Fröbisch (2019), it is likely that the space dorsal to the transverse lamina made up an olfactory chamber, and the large space anterior to the transverse lamina provided a respiratory chamber, which was presumably filled with cartilaginous maxilloturbinals attached to the short ridge running forward beyond the opening of the lacrimal canal (Figs. 4, 5).

The palatines are laterally compressed, resulting in a strong dorsal displacement especially for the left palatine, which almost reaches the nasals (Figs. 5B, 7). Anteriorly, the palatine contacts the maxilla on the secondary palate. Although damaged, the palatine forms much of the floor, lateral wall and roof of the nasopharyngeal passage and part of the posterolateral wall of the olfactory chamber (Figs. 5, 7) (Crompton et al., 2017; Pusch, Kammerer & Fröbisch, 2019). Similar to *Galesaurus* (Pusch, Kammerer & Fröbisch, 2019), the dorsal surface of the palate posterior to the internal choanae consists almost solely

of the palatines, with components of the lacrimal laterally, the jugal posterolaterally and the pterygoid posteriorly and posteromedially (Figs. 5, 7).

As in the case of the vomer and palatines, the preserved portions of the pterygoids are laterally compressed, with the left pterygoid having been stretched as a result of anterior shifting of the left half of the skull, and the right pterygoid having been strongly compressed due to posterior shifting of the right half of the skull. The pterygoid forms the posterior portion of the palate, contacting the narrow posterior end of the vomer and the palatines anteriorly, and the posteroventral extension of the lacrimal and the anterior portion of the jugal anterolaterally. It bears a short transverse flange, which descends far down the medial surface of the dentary, with its ventral tip contacting the anterior portion of the prearticular. An ectopterygoid, which is usually situated at the lateral margin of the transverse flange of the pterygoid, could not be clearly delimited in the scan, but based on the condition in other basal cynodonts is likely to be present (Figs. 4, 7). Despite incompleteness of the posterior portions of the pterygoids, no interpterygoid vacuity seems to be present between them (Fig. 7), potentially indicating maturity in this specimen.

Lower jaw

The lower jaw of BSPG 1934-VIII-7 is tightly occluded to the upper jaw, and has suffered compression comparable to that of the cranium. Anteriorly, the left and right dentaries seem to be fused at the symphysis (Figs. 2, 3, 4, 8, 9). A fused mandibular symphysis, which is typically considered a eucynodont synapomorphy (Hopson & Kitching, 2001), has not yet been described for any cynodont stemward of that clade. Abdala et al. (2019) recently reported a fused mandibular symphysis for the Permian *Vetusodon*, but Huttenlocker & Sidor (2020) doubted the presence of this feature in this taxon and changed the coding of this character to 'absent' in their phylogenetic dataset. In BSPG 1934-VIII-7, a fused symphysis cannot be confirmed with certainty based on external examination, because of damage to the surface in the actual specimen. However, the CT-data (which shows no sign of a suture between the mandibular rami) and the fact that the jaw symphysis has remained in place as a single unit even after distortion (the dentaries frequently dislocate in therapsid skulls showing this style of compression) together provide strong evidence that this structure is fused in *Bolotridon* (Figs. 8, 9).

In lateral view, the dentaries gently curve upwards at the symphysis. They consist of a horizontal, tooth-bearing ramus, with its ventral margin being damaged on the right side, and a posterodorsally sloping coronoid process, which is slightly damaged on both sides. The tip of the coronoid process is located close to the postorbital bar and its posterior margin, which is better preserved on the right side, and slopes posteroventrally to contact the postdentary bones, of which only a portion of the right prearticular is preserved (Figs. 1–4, 8). The dentary houses three incisors (only the left incisor arcade is complete; the second incisor on the right side has fallen out), one canine, and ten postcanines. Both the canine and postcanines in the right dentary are preserved in place. In contrast, the left lower postcanine row is missing pc3 and pc4 and has been slightly shifted inwards due to lateral compression. The left pc1, pc2 and canine are placed somewhat anterior to their counterparts on the right side. As in the upper jaw, there is a short diastema

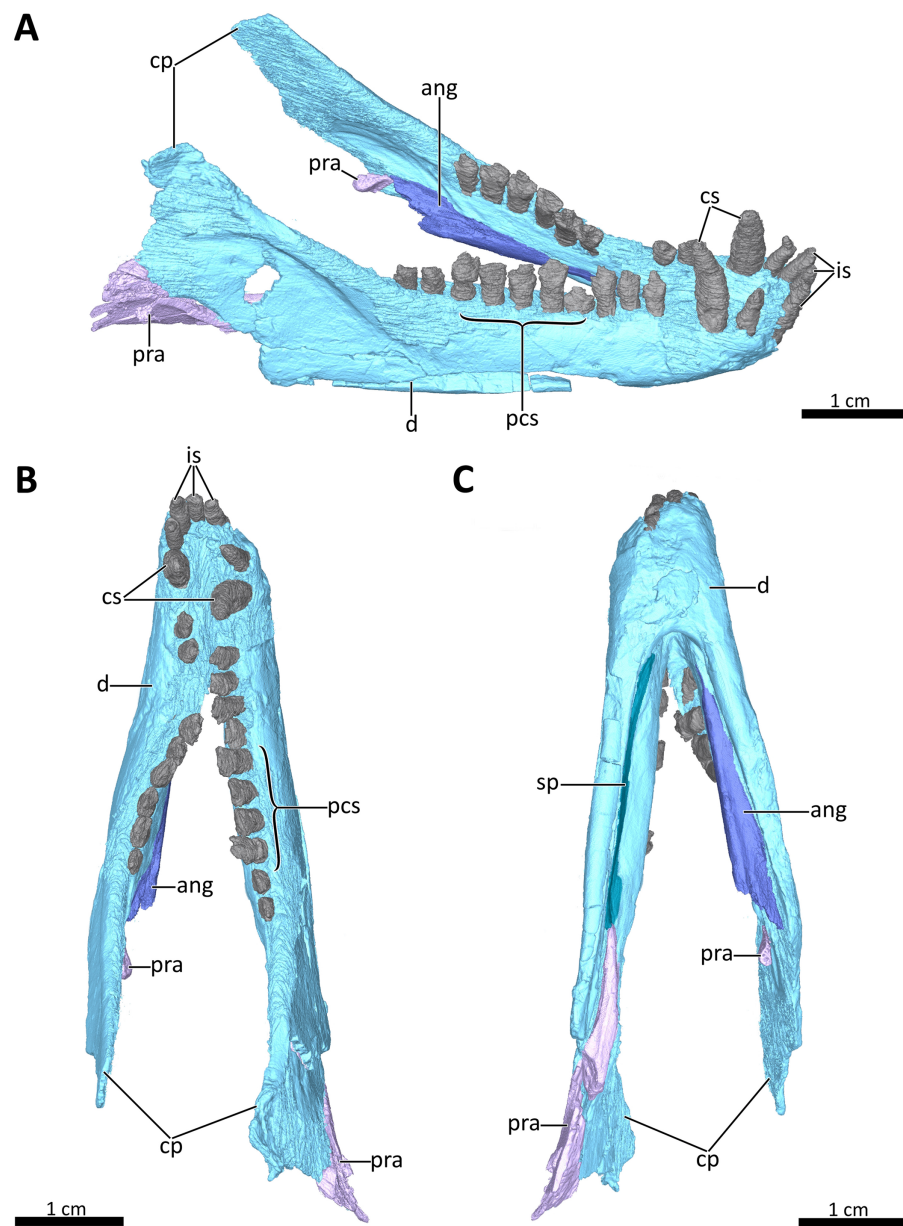


Figure 8 3D reconstruction of the lower jaw of BSPG 1934-VIII-7. (A) Right dorsolateral, (B) dorsal, and (C) ventral view of the mandible. *Abbreviations:* ang, angular; cp, coronoid process; cs, lower canines; d, dentary; is, lower incisors; pcs, lower postcanines; pra, prearticular; sp, splenial. Images in (A), (B) and (C) by Luisa C. Pusch. [Full-size !\[\]\(ebfe6d37ad86655679811e032f633da4_img.jpg\) DOI: 10.7717/peerj.11542/fig-8](https://doi.org/10.7717/peerj.11542/fig-8)

present between the lower canine and first lower postcanine. The lower postcanines are generally poorly preserved, likely due to their appression and subsequent compression against the upper jaw. In the right dentary, both the last and penultimate postcanines are similar in size, but noticeably smaller than the other teeth with the exception of pc4. These two posteriormost teeth and pc4 either have damaged crowns or are not yet fully erupted (Fig. 8). The small holes visible on the ventral surface of the premaxilla just

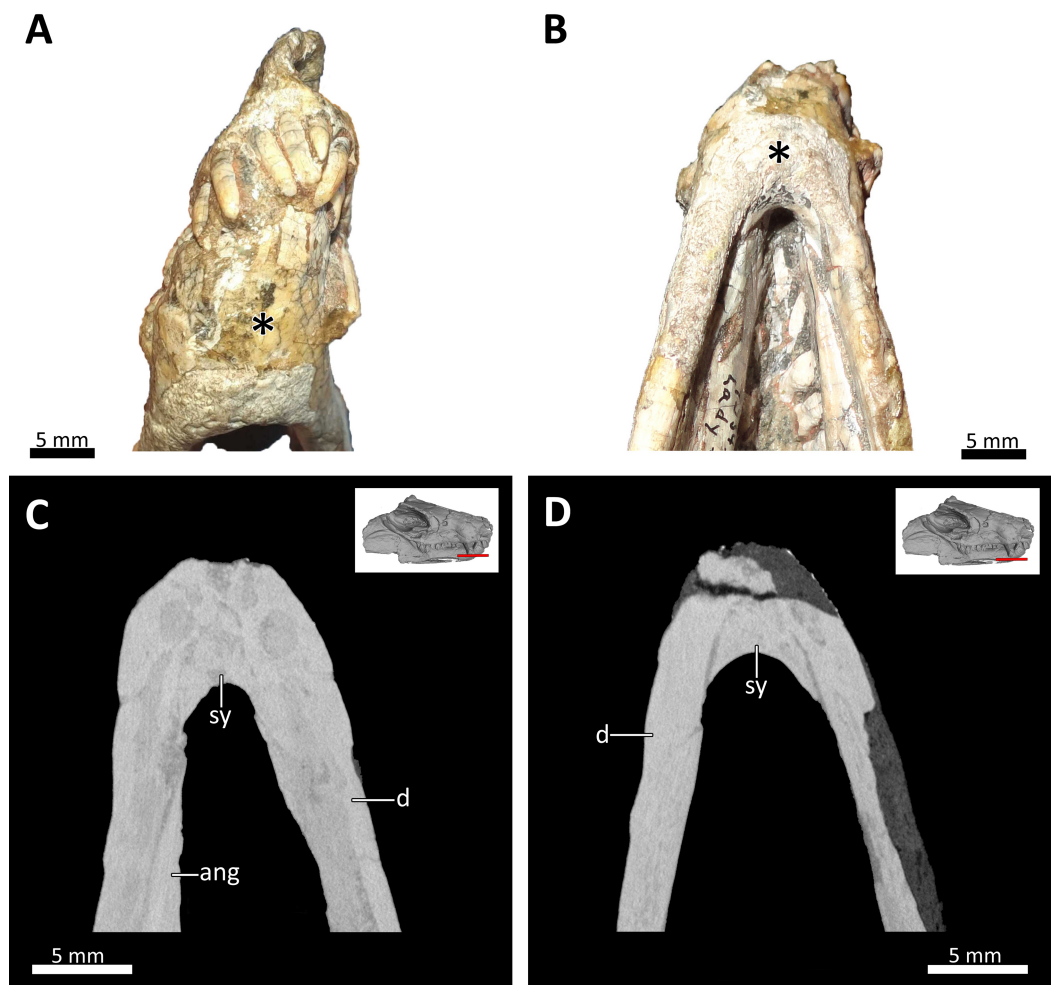


Figure 9 Symphyseal region of BSPG 1934-VIII-7. (A) Anterior and (B) ventral views of the symphyseal region highlighted with an asterisk. (C) and (D) virtual horizontal CT sections through the symphyseal region. Abbreviations: ang, angular; d, dentary; sy, symphysis. Photograph in (A) by Luisa C. Pusch and in (B) by Christian F. Kammerer. CT images in (C) and (D) by Luisa C. Pusch.

Full-size DOI: [10.7717/peerj.11542/fig-9](https://doi.org/10.7717/peerj.11542/fig-9)

posterior to the upper incisor row are likely not caused by taphonomically-induced impression of the lower incisors into the upper jaw, but rather seem to be naturally present to accommodate the crowns of the enlarged lower teeth (Fig. 7B). Such holes for accommodating the lower incisors are also observed on the ventral surface of the premaxilla in *Thrinaxodon* (e.g. [Jasinowski, Abdala & Fernandez, 2015](#): Fig. 7).

A well-developed masseteric fossa for the adductor musculature in the posterior portion of the horizontal ramus of the right dentary extends anteriorly to a point below the anterior margin of the orbit at the level between the last and penultimate upper postcanines, with its anterior and ventral margins being offset from the rest of the dentary by a pronounced lateral curvature around the postdentary bar (Fig. 2A). The definition and extension of the masseteric fossa, as well as the larger coronoid process with its tip being located close to the postorbital bar, closely resemble the condition described for

Thrinaxodon and more derived cynodonts, rather than what is visible in the galesaurids *Progalesaurus* and *Galesaurus* in which the masseteric fossa is not well defined and the coronoid process is not as large, or Permian taxa in which the fossa is restricted to the coronoid process (Kemp, 1979; Abdala & Damiani, 2004; Sidor & Smith, 2004; Ivakhnenko, 2013; Kammerer, 2016; Huttenlocker & Sidor, 2020).

The splenial is present as a thin, anteroposteriorly elongated element positioned medial to the horizontal ramus of the right dentary by which it is completely obscured from lateral view. Anteriorly, it extends from the level of the root of the lower canine, where it contributes to the mandibular symphysis, to a level near the posterior margin of the dentary where it underlies the anterior tip of the prearticular (Figs. 4, 8A, 8C).

The right prearticular is broken and incomplete and only extends up to the posterior margin of the coronoid process. Its anterior portion, which contacts the splenial anteriorly, rests medial to the posterior margin of the dentary where it is overlapped by the ventral tip of the descending transverse flange of the pterygoid (Figs. 2, 4, 8).

The angular, which usually forms the ventral and posterolateral portion of the lower jaw, is also broken and incompletely preserved in BSPG 1934-VIII-7. Its anterior portion, which is only preserved on the left side, has been strongly shifted anteriorly extending medially along the tooth-bearing horizontal ramus of the dentary. An articular facet is visible on its posterodorsal surface to accommodate the prearticular, which is (with the exception of a small fragment) not preserved on the left side. The reflected lamina of the angular is completely missing in this specimen (Fig. 8).

DISCUSSION

Phylogeny of early cynodonts

The parsimony analysis recovered 24 most parsimonious trees with a tree length of 256 (consistency index = 0.598, retention index = 0.809). Generally, the strict consensus and Bayesian inference majority rule topologies (Fig. 10) are similar to those of Huttenlocker & Sidor (2020), but the interrelationships of epicynodonts in our parsimony analysis are better resolved after including *Bolotridon*. Topology for non-epicynodont cynodonts is identical to that of Huttenlocker & Sidor (2020), with charassognathids and *Dvinia* recovered in a clade at the base of Cynodontia and *Procynosuchus* crownward of them.

As in the earlier analysis, *Abdalodon diastematicus* and *Nshimbodon muchingaensis* are recovered as sister-taxa with extremely high support. These two taxa, the former known from a small, dorsoventrally crushed skull from the South African *Endothiodon* AZ and the latter from a relatively well-preserved skull from the Zambian Madumabisa Mudstone Formation, are exceedingly similar, and the diagnostic features of the latter cited by Huttenlocker & Sidor (2020) are all questionable. These authors differentiated *Nshimbodon* from *Abdalodon* by a gentler anteroventral slope of the rostrum and proportionally deeper dentary ramus. However, the diagnostic value of these characters is rendered dubious by extreme dorsoventral compression in the holotype of *A. diastematicus*, which has altered the snout profile and relative height of the dentary. Potential ontogenetic variation in jaw robusticity also should be considered, as the holotype of *A. diastematicus* represents a somewhat smaller specimen (5.61 cm skull

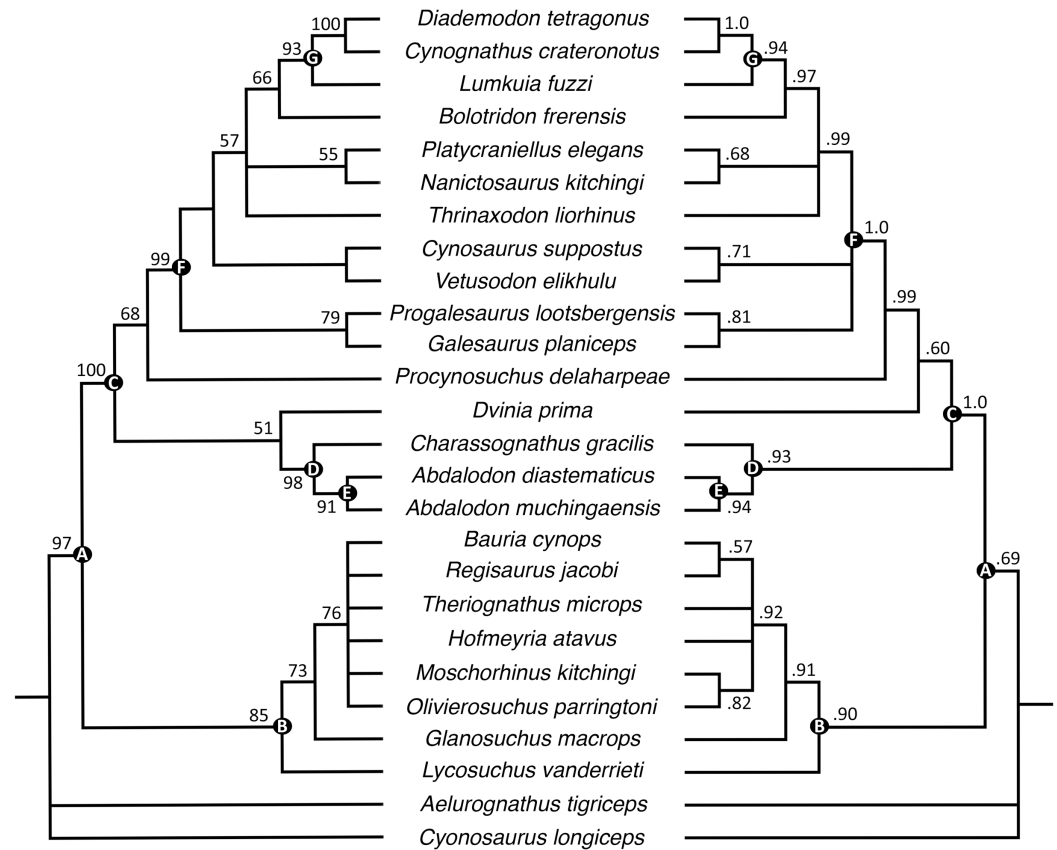


Figure 10 Maximum parsimony strict consensus (left) and Bayesian inference majority rule (right) topologies of Permo-Triassic theriodonts obtained from the phylogenetic analyses. Nodes of clades of interest are labeled: (A) Eutheriodontia; (B) Therocephalia; (C) Cynodontia; (D) Charassognathidae; (E) Abdalodontinae; (F) Epicynodontia; (G) Eucynodontia. Numbers at nodes represent clade support, if no bootstrap value is indicated on the left it was less than 50%, and Bayesian posterior probabilities on the right. Image by Luisa C. Pusch. [Full-size !\[\]\(78455399e1afe561232b644638671568_img.jpg\) DOI: 10.7717/peerj.11542/fig-10](https://doi.org/10.7717/peerj.11542/fig-10)

length) than that of *N. muchingaensis* (7.0 cm). Other listed autapomorphies for *Nshimbodon* include tooth count and the presence of a series of neurovascular pits on the dentary, but in these features it accords closely with *Abdalodon* (Kammerer, 2016). Here, we synonymize *Nshimbodon* with *Abdalodon*, albeit tentatively retaining the species *muchingaensis* considering geographic and probable stratigraphic separation from *A. diastematicus*. Additional specimens from Zambia and South Africa will be required to determine whether even specific separation is warranted.

As in the analyses of Huttenlocker & Sidor (2020), Epicynodontia and Eucynodontia are recovered with strong support in our analyses. The strict consensus tree recovers the Triassic galesaurids *Galesaurus* and *Progalesaurus* at the base of Epicynodontia, followed by the Permian *Cynosaurus* (sometimes considered a galesaurid) and *Vetusodon*, here in a sister-taxon relationship and occupying a position crownward of the latter taxa. This contrasts with the strict consensus of Huttenlocker & Sidor (2020), in which the majority of non-eucynodont epicynodont taxa form an unresolved polytomy. In our Bayesian tree, galesaurids and *Vetusodon* + *Cynosaurus* form an unresolved polytomy at

the base of Epicynodontia as in the Bayesian tree of [Huttenlocker & Sidor \(2020\)](#). The slightly more crownward position of *Cynosaurus* in our strict consensus tree differs from what was suggested by previous workers, who recovered *Cynosaurus* as stemward to *Galesaurus* and *Progalesaurus* (e.g., [Abdala, 2007](#); [Kammerer, 2016](#); [Van den Brandt & Abdala, 2018](#); [Abdala et al., 2019](#)), but this position lacks unambiguous apomorphies supporting it. The clade formed by *Vetusodon* and *Cynosaurus* is recovered with low support in our parsimony analysis, but modest support in the Bayesian analysis.

Both the parsimony and Bayesian analyses recover *Bolotridon* as the sister-taxon of Eucynodontia ([Fig. 10](#)). *Thrinaxodon* is recovered in a polytomy with *Nanictosaurus* + *Platycraniellus* and *Bolotridon* + Eucynodontia in both analyses. The clade uniting *Bolotridon* + Eucynodontia has modest support in the parsimony analysis, but is recovered with strong support in the Bayesian analysis, despite many unknown characters as a result of the physical incompleteness of BSPG 1934-VIII-7. Evidence for a sister-taxon relationship between *Bolotridon* and Eucynodontia is provided by only a single but very important character: fusion of the mandibular symphysis, which was historically considered a eucynodont synapomorphy ([Hopson & Kitching, 2001](#)). A position outside of Eucynodontia is supported by the morphology of the dentary symphysis, which is low and gently sloping in *Bolotridon*, as in more stemward cynodonts. In eucynodonts the dentary symphysis is tall, steeply-sloped and forms a distinct 'chin'. A similar morphology was also described for the dentary symphysis of the Permian *Vetusodon* and *Cynosaurus*, but this is here optimized as convergence (e.g., [Van den Brandt & Abdala, 2018](#); [Abdala et al., 2019](#); [Huttenlocker & Sidor, 2020](#): Supplemental Information).

Comparison of *Bolotridon* with other cynodonts

The new data obtained from the CT-scan permit a better resolved position for *Bolotridon* than in the phylogenetic analysis of [Sidor & Smith \(2004\)](#), where it was nested in a polytomy with Galesauridae and a clade consisting of the more derived epicynodonts *Thrinaxodon* and *Platycraniellus*. Inclusion of *Bolotridon* in Galesauridae is not supported by our results. In addition to a fused mandibular symphysis, which is not known from any late Permian or Early Triassic cynodont, a crownward position for *Bolotridon* relative to the galesaurids is supported by three additional characters in our analysis. One of these characters uniting *Bolotridon* with the more derived epicynodonts *Thrinaxodon*, *Nanictosaurus*, *Platycraniellus*, and eucynodonts to the exclusion of galesaurids is the presence of a well-developed masseteric fossa extending to the angle of the horizontal ramus of the dentary. The other two characters show a more complex distribution, being shared with the crownward epicynodonts *Thrinaxodon* and *Nanictosaurus* but also stemward Permian cynodonts, and not with eucynodonts or galesaurids. These are the absence of a strongly recurved main cusp on the posterior postcanines (the presence of this character in *Progalesaurus* and *Galesaurus* is interpreted as having evolved convergently from eucynodonts ([Huttenlocker & Sidor, 2020](#): Supplemental Information)) and the presence of a lingual cingulum in the lower postcanines. The absence of this feature in the lower postcanines of *Progalesaurus* and *Galesaurus* might have evolved independently

from eucynodonts as well, but since this character is so far uncertain in *Vetusodon*, *Cynosaurus*, and Charassognathidae, this cannot be confirmed.

Although endocranial characters have been described for various therapsids in CT-assisted studies in recent years, with special focus on cynodonts as the therapsid clade ancestral to (and including) mammals (e.g., [Hillenius, 1994](#); [Kemp, 2009](#); [Rodrigues, Ruf & Schultz, 2013, 2014](#); [Rodrigues et al., 2018](#); [Benoit, Manger & Rubidge, 2016](#); [Benoit et al., 2017a, 2017b, 2017c, 2018, 2019](#); [Araújo et al., 2017, 2018](#); [Crompton, Musinsky & Owerkowicz, 2015](#); [Crompton et al., 2017](#); [Bendel et al., 2018](#); [Pusch, Kammerer & Fröbisch, 2019](#); [Pusch et al., 2020](#); [Huttenlocker & Sidor, 2020](#)), they still remain understudied compared to the well-known external craniodental features in synapsids and thus have been largely ignored in phylogenetic analyses. The data matrix of [Huttenlocker & Sidor \(2020\)](#) is the only matrix so far including newly adapted information from [Benoit et al. \(2017a\)](#) about the rarely preserved orbitosphenoid in therapsids. Despite damage and incomplete preservation of BSPG 1934-VIII-7, we were able to describe a few endocranial characters for *Bolotridon* that are consistent with an epicynodont position for this taxon. Those characters include a maxillary canal that would have arisen from a relatively small maxillary antrum (antrum visible in CT-scan, but canal itself not resolvable due to damage) and a possible maxilloturbinal ridge extending forward beyond the opening of the lacrimal. The presence of the latter is rendered somewhat uncertain by poor preservation and CT-resolution in this region of the snout; as mentioned in our description a ridge appears to be present but could also represent a crack. Ridges that would have served as attachment point for cartilaginous maxilloturbinals have been described so far only for the epicynodonts *Galesaurus* and *Thrinaxodon* and for eucynodonts such as the cynognathian *Massetognathus* and the probainognathian *Probainognathus* ([Crompton, 2013](#); [Crompton, Musinsky & Owerkowicz, 2015](#); [Crompton et al., 2017](#); [Pusch, Kammerer & Fröbisch, 2019](#)); they are absent in the non-epicynodonts *Abdalodon muchingaensis* ([Huttenlocker & Sidor, 2020](#)) and *Procynosuchus delaharpeae* ([Kemp, 1979](#)). Based on its position crownward of *Galesaurus* and *Thrinaxodon* in our analysis, presence of a maxilloturbinal ridge can be inferred for *Bolotridon*, even if the current record is less than definitive. A relatively small maxillary antrum from which the branching maxillary canal extends forward has also been described for *Galesaurus* and *Thrinaxodon* and is additionally present in basal probainognathian eucynodonts such as *Ecteninion* and *Lumkuia*. This contrasts with what is observed in the cynognathians *Trirachodon* and *Massetognathus*, in which the antrum is massive by comparison, and more crownward probainognathians, in which the maxillary antrum is separated from the maxillary canal and resembles the mammaliaform pattern ([Benoit, Manger & Rubidge, 2016](#); [Benoit et al., 2019](#); [Crompton et al., 2017](#); [Pusch, Kammerer & Fröbisch, 2019](#)).

However, data concerning the morphology of the maxillary canal and antrum of cynodonts stemward of *Galesaurus* are still lacking, so it is uncertain whether a relatively small antrum represents a derived condition among early cynodonts or if this feature is conservative among basal taxa of this clade. Denser sampling of endocranial

features of basal cynodonts is needed to test where this and other mammalian features might have first evolved.

A unique fauna of small-bodied therapsids in the *Trirachodon-Kannemeyeria* Subzone

The *Trirachodon-Kannemeyeria* Subzone of the *Cynognathus* AZ is the most fossil- and species-rich of the three *Cynognathus* AZ subzones. Therapsids in this subzone are represented by the abundant dicynodont *Kannemeyeria simocephalus*, the rare therocephalians *Microgomphodon oligocynus* and *Bauria cynops*, and cynodonts such as the common *Cynognathus crateronotus*, *Diademodon tetragonus*, *Trirachodon berryi*, and *Trirachodon/Cricodon kannemeyeri* (the latter first appearing at the top of this subzone) ([Abdala, Hancox & Neveling, 2005](#); [Abdala & Ribeiro, 2010](#); [Smith, Rubidge & Van der Walt, 2012](#): Table 2.5; [Hancox, Neveling & Rubidge, 2020](#)). In addition to the usual occurrences of *Trirachodon*, *Cynognathus*, *Diademodon*, and *Kannemeyeria* at Lady Frere, this area (consisting of both the Commonage and nearby localities like Lumku Mission in Chris Hani District Municipality) yields unique records of small-bodied therapsid taxa including the dicynodont *Kombuisia frerensis*, the basal cynodont *Bolotridon frerensis*, and the early probainognathian *Lumkuia fuzzi* ([Broili & Schröder, 1934](#); [Kitching, 1963](#); [Hotton, 1974](#); [Hopson & Kitching, 2001](#); [Fröbisch, 2007](#); [Abdala, Hancox & Neveling, 2005](#); [Abdala & Ribeiro, 2010](#); [Smith, Rubidge & Van der Walt, 2012](#): Table 2.5; [Hancox, Neveling & Rubidge, 2020](#)).

These seemingly anachronistic faunal elements (representing both ‘relict’ taxa like the emydopoid dicynodont *Kombuisia* and the non-eucynodont *Bolotridon*, and an early representative of the later-radiating cynodont clade Probainognathia in *Lumkuia*) highlight the complex and transitional nature of the *Cynognathus* AZ fauna. Gaps in our knowledge of small-bodied taxa throughout the Triassic make confident evaluation of the stratigraphic ranges of some groups difficult, complicating our understanding of what is truly ‘relictual’ vs. just rarely preserved. For example, the cynodonts *Bolotridon* and *Lumkuia* are not known from localities outside of the area surrounding Lady Frere, and are restricted to the *Trirachodon-Kannemeyeria* Subzone of the *Cynognathus* AZ. The type species of the rare dicynodont *Kombuisia* (*K. frerensis*), which is only known from two specimens from the Lady Frere locality, is also restricted to the *Trirachodon-Kannemeyeria* Subzone of the *Cynognathus* AZ. However, a second species of the genus, *Kombuisia antarctica* from the lower Fremouw Formation in Antarctica, extends the known stratigraphic range of *Kombuisia* into rocks that are equivalent in age to the Lower Triassic *Lystrosaurus declivis* AZ of South Africa ([Fröbisch, 2007](#); [Fröbisch, Angielczyk & Sidor, 2010](#); [Botha & Smith, 2020](#); [Hancox, Neveling & Rubidge, 2020](#)).

It is possible that the apparent restriction of these taxa to the area surrounding Lady Frere is an artifact of unusual preservational conditions; something lending itself to the preservation of small-bodied, rare taxa not recorded at other *Cynognathus* AZ localities. Complicating this interpretation somewhat is the broader geographic range of certain otherwise-comparable coeval therapsids. The bauriid *Bauria* is also relatively small (basal skull length ~12 cm), is in some ways a ‘relict’ (being among the geologically youngest

therocephalians), and occurs only in the *Trirachodon-Kannemeyeria* Subzone, but is much more widely distributed across the Karoo Basin (*Kitching, 1963; Abdala et al., 2014; Hancox, Neveling & Rubidge, 2020*). Another contemporaneous bauriid, *Microgomphodon*, exhibits substantially broader stratigraphic and geographic ranges, occurring from the lower *Langbergia-Garjainia* Subzone to the *Trirachodon-Kannemeyeria* Subzone in the South African *Cynognathus* AZ and also the upper Omingonde Formation of Namibia (*Abdala et al., 2014; Hancox, Neveling & Rubidge, 2020*). The greatest geographic and stratigraphic range for a *Cynognathus* AZ tetrapod, however, is that of the small parareptile *Palacrodon browni*. Originally known from the *Cynognathus* AZ of South Africa, this taxon was later discovered in the lower Fremouw Formation of Antarctica (which correlates chronostratigraphically with the Lower Triassic *Lystrorhynchus declivis* AZ of South Africa) and the Upper Triassic Chinle Formation of northeastern Arizona, USA (*Kligman, Marsh & Parker, 2018; Botha & Smith, 2020; Hancox, Neveling & Rubidge, 2020*). The presence of *Palacrodon* in the middle Norian of the southwest United States extends the stratigraphic range of this genus by at least 15 million years, indicating remarkable persistence. Taken as a whole, these examples suggest that small-bodied Triassic tetrapods are greatly undersampled in the record. This is particularly likely to bias local estimates of diversity and richness, where localities may record the most abundant small-bodied taxa (e.g., trirachodontid cynodonts in the *Cynognathus* AZ), but with rarer small-bodied members of these assemblages unlikely to be preserved and/or collected. This is well-illustrated by the extreme paucity of known *Palacrodon* fossils, despite its stratigraphic duration of ~35 million years and Pangean distribution, and accentuated by the fact that the survival of emydopoid dicynodonts and non-eucynodont cynodonts into the Middle Triassic would be completely unknown if not for the exceptional record at Lady Frere. What makes this site exceptional is currently uncertain; whether the paleoenvironment favored by *Kombuisia* and *Bolotridon* was not present in other *Cynognathus* AZ localities, whether local depositional environments favored preservation of small-bodied animals, or whether some combination of these and/or collection bias explains its unusual local fauna is uncertain. Most of the published records from the area are from historical collections, and new, detailed lithological and stratigraphical studies are needed to understand the local environment and preservational regime in order to get answers.

CONCLUSIONS

Our redescription of the enigmatic basal cynodont *Bolotridon frerensis*, based on a computed tomographic (CT) reconstruction of the specimen BSPG 1934-VIII-7, provides new information on the palatal region and endocranial characters of this taxon that were previously obscured. Despite damage to the cranium, we were able to recognize several seemingly advanced craniodental characters shared with cynodonts more derived than galesaurids, including a well-developed masseteric fossa extending to the angle of the horizontal ramus of the dentary, a feature shared with more crownward epicynodonts such

as *Thrinaxodon* and eucynodonts. Our recognition of a possibly fused mandibular symphysis in this taxon also supports a relatively crownward position for *Bolotridon*. The recovery of *Bolotridon* as the sister-taxon of Eucynodontia in both of our analyses indicates that while this taxon may be something of a relict, being from an earlier divergence than its contemporaries *Cynognathus*, *Trirachodon*, *Diademodon* and *Lumkuia* (Hancox, Neveling & Rubidge, 2020), it is not quite the *Thrinaxodon*-grade primordial cynodont that some previous authors have argued (e.g., Battail, 1991). It nevertheless represents part of an unusual assemblage for its time, and indicates that substantial diversity among Triassic taxa at small body size is likely currently unknown. Although this may in large part reflect real preservational bias, additional worker effort even in well-studied assemblages like the *Cynognathus* AZ is necessary, particularly at sites like Lady Frere known to produce rare, small-bodied taxa.

INSTITUTIONAL ABBREVIATIONS

- BSPG** Bayerische Staatssammlung für Paläontologie und Geologie, Munich, Germany.
- NHMUK PV** Natural History Museum, Vertebrate Palaeontological Collection, London, UK.

ACKNOWLEDGEMENTS

We wish to thank Oliver Rauhut (Bayerische Staatssammlung für Paläontologie und Geologie, Munich, Germany) for the loan of BSPG 1934-VIII-7 and Kristin Mahlow (CT-Laboratory, Museum für Naturkunde, Berlin, Germany) for scanning the specimen. LCP would like to thank Mark MacDougall (Museum für Naturkunde, Berlin, Germany) and Neil Brocklehurst (University of Oxford, United Kingdom) for their brief introductions into PAUP* and MrBayes. Furthermore, we would like to thank Ken Angielczyk and Jim Hopson for their thorough and constructive reviews of the manuscript and Brandon Hedrick for work as editor.

ADDITIONAL INFORMATION AND DECLARATIONS

Funding

This work was supported by a grant from the Deutsche Forschungsgemeinschaft (FR 2457/8-1) to Jörg Fröbisch. The funders had no role in study design, data collection and analysis, decision to publish, or preparation of the manuscript.

Grant Disclosures

The following grant information was disclosed by the authors:
Deutsche Forschungsgemeinschaft: (FR 2457/8-1).

Competing Interests

The authors declare that they have no competing interests.

Author Contributions

- Luisa C. Pusch conceived and designed the experiments, performed the experiments, analyzed the data, prepared figures and/or tables, authored or reviewed drafts of the paper, and approved the final draft.
- Christian F. Kammerer conceived and designed the experiments, performed the experiments, authored or reviewed drafts of the paper, contributed reagents/materials/analysis tools, and approved the final draft.
- Jörg Fröbisch performed the experiments, authored or reviewed drafts of the paper, contributed reagents/materials/analysis tools, and approved the final draft.

Data Availability

The following information was supplied regarding data availability:

Raw CT scans are available at the Data Repository of the Museum für Naturkunde Berlin: DOI [10.7479/qcjm-dv44](https://doi.org/10.7479/qcjm-dv44).

The data matrix and character list used in the phylogenetic analyses are available in the [Supplemental Files](#).

Supplemental Information

Supplemental information for this article can be found online at <http://dx.doi.org/10.7717/peerj.11542#supplemental-information>.

REFERENCES

- Abdala F. 2007.** Redescription of *Platycraniellus elegans* (Therapsida, Cynodontia) from the lower Triassic of South Africa, and the cladistic relationships of eutheriodonts. *Palaeontology* **50**(3):591–618 DOI [10.1111/j.1475-4983.2007.00646.x](https://doi.org/10.1111/j.1475-4983.2007.00646.x).
- Abdala F, Allinson M. 2005.** The taxonomic status of *Parathrinaxodon proops* (Therapsida: Cynodontia), with comments on the morphology of the palate in basal cynodonts. *Palaeontologia Africana* **41**:45–52.
- Abdala F, Giannini N. 2002.** Chiniquodontid cynodonts: systematic and morphometric considerations. *Palaeontology* **45**(6):1151–1170 DOI [10.1111/1475-4983.00280](https://doi.org/10.1111/1475-4983.00280).
- Abdala F, Damiani R. 2004.** Early development of the mammalian superficial masseter muscle in cynodonts. *Paleontologia Africana* **40**:23–29.
- Abdala F, Ribeiro AM. 2010.** Distribution and diversity patterns of Triassic cynodonts (Therapsida, Cynodontia) in Gondwana. *Paleogeography, Paleoclimatology, Paleoecology* **286**(2–3):202–217 DOI [10.1016/j.palaeo.2010.01.011](https://doi.org/10.1016/j.palaeo.2010.01.011).
- Abdala F, Hancox PJ, Neveling J. 2005.** Cynodonts from the uppermost Burgersdorp Formation, South Africa, and their bearing on the biostratigraphy and correlation of the Triassic *Cynognathus* Assemblage Zone. *Journal of Vertebrate Paleontology* **25**(1):192–199 DOI [10.1671/0272-4634\(2005\)025\[0192:CFTUBF\]2.0.CO;2](https://doi.org/10.1671/0272-4634(2005)025[0192:CFTUBF]2.0.CO;2).
- Abdala F, Jasinowski S, Fernandez V. 2013.** Ontogeny of the Early Triassic cynodont *Thrinaxodon liorhinus* (Therapsida): dental morphology and replacement. *Journal of Vertebrate Paleontology* **33**(6):1408–1431 DOI [10.1080/02724634.2013.775140](https://doi.org/10.1080/02724634.2013.775140).
- Abdala F, Gaetano LC, Smith RMH, Rubidge BS. 2019.** A new large cynodont from the late Permian (Lopingian) of the South African Karoo Basin and its phylogenetic significance. *Zoological Journal of the Linnean Society* **186**(4):983–1005 DOI [10.1093/zoolinnean/zlz004](https://doi.org/10.1093/zoolinnean/zlz004).

- Abdala F, Jashashvili T, Rubidge BS, van den Heever J. 2014.** New material of *Microgomphodon oligocynus* (Eutherapsida, Therocephalia) and the taxonomy of southern African Bauriidae. In: Kammerer CF, Angielczyk KD, Fröbisch J, eds. *Early Evolutionary History of the Synapsida*. Dordrecht: Springer, 209–231.
- Angielczyk KD, Kammerer CF. 2018.** Non-Mammalian synapsids: the deep roots of the mammalian family tree. In: Zachos FE, Asher RJ, eds. *Handbook of Zoology: Mammalian Evolution, Diversity and Systematics*. Berlin/Boston: Walter de Gruyter GmbH & Co. KG, 117–198.
- Araújo RM, Fernandez V, Polcyn MJ, Fröbisch J, Martins RMS. 2017.** Aspects of gorgonopsian paleobiology and evolution: insights from the basicranium, occiput, osseous labyrinth, vasculature, and neuroanatomy. *PeerJ* 5(1):e3119 DOI 10.7717/peerj.3119.
- Araújo RM, Fernandez V, Rabbitt RD, Ekdale EG, Antunes MT, Castanhinha R, Fröbisch J, Martins RMS. 2018.** *Endothiodon* cf. *bathystoma* (Synapsida: Dicynodontia) bony labyrinth anatomy, variation and body mass estimates. *PLOS ONE* 13(3):e0189883 DOI 10.1371/journal.pone.0189883.
- Battail B. 1991.** Les cynodontes (Reptilia, Therapsida): une phylogénie. *Bulletin du Muséum d'histoire naturelle* 13:17–105.
- Bendel E-M, Kammerer CF, Kardjilov N, Fernandez V, Fröbisch J. 2018.** Cranial anatomy of the gorgonopsian *Cynariops robustus* based on CT-reconstruction. *PLOS ONE* 13(11):e0207367 DOI 10.1371/journal.pone.0207367.
- Benoit J, Angielczyk KD, Miyamae JA, Manger P, Fernandez V, Rubidge B. 2018.** Evolution of facial innervation in anomodont therapsids (Synapsida): insights from X-ray computerized microtomography. *Journal of Morphology* 279(5):1–29 DOI 10.1002/jmor.20804.
- Benoit J, Jasinoski SC, Fernandez V, Abdala F. 2017a.** The mystery of a missing bone: revealing the orbitosphenoid in basal Epicynodontia (Cynodontia, Therapsida) through computed tomography. *The Science of Nature* 104(7–8):66 DOI 10.1007/s00114-017-1487-z.
- Benoit J, Manger PR, Fernandez V, Rubidge BS. 2017b.** The bony labyrinth of the late Permian Biarmosuchia: palaeobiology and diversity in non-mammalian Therapsida. *Palaeontologia Africana* 52:58–77.
- Benoit J, Manger PR, Norton L, Fernandez V, Rubidge BS. 2017c.** Synchrotron scanning reveals the paleoneurology of the head-butting *Moschops capensis* (Therapsida, Dinocephalia). *PeerJ* 5(8):e3496 DOI 10.7717/peerj.3496.
- Benoit J, Manger PR, Rubidge BS. 2016.** Palaeoneurological clues to the evolution of defining mammalian soft tissue traits. *Scientific Reports* 6(1):25604 DOI 10.1038/srep25604.
- Benoit J, Ruf I, Miyamae JA, Fernandez V, Rodrigues PG, Rubidge BS. 2019.** The evolution of the maxillary canal in probainognathia (Cynodontia, Synapsida): reassessment of the homology of the infraorbital foramen in mammalian ancestors. *Journal of Mammalian Evolution* 27(3):1–20 DOI 10.1007/s10914-019-09467-8.
- Botha J, Smith RMH. 2020.** Biostratigraphy of the *Lystrosaurus declivis* Assemblage Zone (Beaufort, Group, Karoo Supergroup), South Africa. *South African Journal of Geology* 123(2):207–216 DOI 10.25131/sajg.123.0015.
- Botha J, Abdala F, Smith RMH. 2007.** The oldest cynodont: new clues on the origin and diversification of the Cynodontia. *Zoological Journal of the Linnean Society* 149(3):477–492 DOI 10.1111/j.1096-3642.2007.00268.x.
- Brink AS, Kitching JW. 1953.** On some new *Cynognathus* zone specimens. *Palaeontologia Africana* 1:29–48.

- Broili F, Schröder J. 1934.** Beobachtungen an Wirbeltieren der Karrooformation. II. Über den Cynodontier *Tribolodon frerensis* Seeley. *Sitzungsberichte der Bayerischen Akademie der Wissenschaften, Sonderdruck aus dem Jahrgang 1934* 163–177.
- Broom R. 1937.** A further contribution to our knowledge of the fossil reptiles of the Karroo. *Proceedings of the Zoological Society of London B* 107:299–318.
- Coad BW. 1977.** On the nomenclature of the genus name *Tribolodon* (Osteichthyes and Reptilia). *Journal of Paleontology* 51:1046–1047.
- Crompton AW. 2013.** Evolution of the mammalian nose, presentation. Available at <https://crompton.oeb.harvard.edu/evolution-mammalian-nose-presentation> (accessed 10 November 2020).
- Crompton AW, Musinsky C, Owerkowicz T. 2015.** Evolution of the mammalian nose. In: Dial K, Shubin N, Brainerd E, eds. *Great Transformations in Vertebrate Evolution*. Chicago: University of Chicago Press, 189–203.
- Crompton AW, Owerkowicz T, Bhullar B-AS, Musinsky C. 2017.** Structure of the nasal region of nonmammalian cynodonts and mammaliaforms: speculations on the evolution of mammalian endothermy. *Journal of Vertebrate Paleontology* 37(1):e126911 DOI 10.1080/02724634.2017.1269116.
- Fourie S. 1974.** The cranial morphology of *Thrinaxodon liorhinus* Seeley. *Annals of the South African Museum* 65:337–400.
- Fröbisch J. 2007.** The cranial anatomy of *Kombuisia frerensis* Hotton (Synapsida, Dicynodontia) and a new phylogeny of anaomodont therapsids. *Zoological Journal of the Linnean Society* 150(1):117–144 DOI 10.1111/j.1096-3642.2007.00285.x.
- Fröbisch J, Angielczyk KD, Sidor CA. 2010.** The Triassic dicynodont *Kombuisia* (Synapsida, Anomodontia) from Antarctica, a refuge from the terrestrial Permian-Triassic mass extinction. *Naturwissenschaften* 97(2):187–196 DOI 10.1007/s00114-009-0626-6.
- Hancox PJ, Neveling J, Rubidge BS. 2020.** Biostratigraphy of the *Cynognathus* Assemblage Zone (Beaufort Group, Karoo Supergroup), South Africa. *South African Journal of Geology* 123(2):217–238 DOI 10.25131/sajg.123.0016.
- Hendrickx C, Gaetano LC, Choiniere JN, Mocke H, Abdala F. 2020.** A new traversodontid cynodont with a peculiar postcanine dentition from the Middle/Late Triassic of Namibia and dental evolution in basal gomphodonts. *Journal of Systematic Paleontology* 18(20):1669–1706 DOI 10.1080/14772019.2020.1804470.
- Hillenius WJ. 1994.** Turbinates in therapsids: evidence for Late Permian origins of mammalian endothermy. *Evolution* 48(2):207–229 DOI 10.1111/j.1558-5646.1994.tb01308.x.
- Hillenius WJ. 2000.** Septomaxilla of nonmammalian synapsids: soft-tissue correlates and a new functional interpretation. *Journal of Morphology* 245:29–50 DOI 10.1002/1097-4687(200007)245:1<29::AID-JMOR3>3.0.CO;2-B.
- Hopson JA. 1991.** Systematics on the nonmammalian Synapsida and implications for patterns of evolution in synapsids. In: Schultze H-P, Trueb L, eds. *Origins of the Higher Groups of Tetrapods: Controversy and Consensus*. Ithaca, NY: Comstock Publishing Associates, 635–693.
- Hopson JA, Kitching JW. 1972.** A revised classification of cynodonts (Reptilia; Therapsida). *Palaeontologia Africana* 14:71–85.
- Hopson JA, Kitching JW. 2001.** A probainognathian cynodont from South Africa and the phylogeny of nonmammalian cynodonts. *Bulletin of the Museum of Comparative Zoology* 156(1):5–35.
- Hotton N. 1974.** A new dicynodont (Reptilia, Therapsida) from *Cynognathus* Zone deposits of South Africa. *Annals of the South African Museum* 64:157–165.

- Huttenlocker AK, Sidor CA. 2020.** A basal nonmammaliaform cynodont from the Permian of Zambia and the origins of mammalian endocranial and postcranial anatomy. *Journal of Vertebrate Paleontology* e1827413(5):e1827413 DOI 10.1080/02724634.2020.1827413.
- Ivakhnenko MF. 2013.** Cranial morphology of *Dvinia prima* Amalitzky (Cynodontia, Thermomorpha). *Paleontological Journal* 47(2):210–222 DOI 10.1134/S0031030113010048.
- Jasinoski SC, Abdala F, Fernandez V. 2015.** Ontogeny of the early Triassic cynodont *Thrinaxodon liorhinus* (Therapsida): cranial morphology. *The Anatomical Record* 298(8):1440–1464 DOI 10.1002/ar.23116.
- Kammerer CF. 2016.** A new taxon of cynodont from the *Tropidostoma* Assemblage Zone (Upper Permian) of South Africa, and the early evolution of Cynodontia. *Papers in Palaeontology* 2(3):387–397 DOI 10.1002/spp2.1046.
- Kammerer CF. 2017.** Anatomy and relationships of the South African gorgonopsian *Arctops* (Therapsida, Theriodontia). *Papers in Paleontology* 3(4):583–611 DOI 10.1002/spp2.1094.
- Kemp TS. 1979.** The primitive cynodont *Procynosuchus*: functional anatomy of the skull and relationships. *Philosophical Transactions of the Royal Society of London B* 285(1005):73–122 DOI 10.1098/rstb.1979.0001.
- Kemp TS. 2005.** *The origin and evolution of mammals*. New York: Oxford University Press.
- Kemp TS. 2010.** The endocranial cavity of a nonmammalian eucynodont, *Chiniquodon thetonicus*, and its implications for the origin of the mammalian brain. *Journal of Vertebrate Paleontology* 29(4):1188–1198 DOI 10.1671/039.029.0430.
- Kitching JW. 1963.** Notes on some fossil pockets and bone beds in the *Cynognathus*-Zone in the Burghersdorp and Lady Frere districts. *Paleontologia Africana* 8:113–118.
- Kligman BT, Marsh AD, Parker WG. 2018.** First record of diapsid *Palacrodon* from the Norian, Late Triassic Chinle Formation of Arizona, and their biogeographic implications. *Acta Palaeontologica Polonica* 63(1):117–127 DOI 10.4202/app.00426.2017.
- Lewis PO. 2001.** A likelihood approach to estimating phylogeny from discrete morphological character data. *Systematic Biology* 50(6):913–925 DOI 10.1080/106351501753462876.
- Lukic-Walther M, Brocklehurst N, Kammerer CF, Fröbisch J. 2019.** Diversity patterns of nonmammalian cynodonts (Synapsida, Therapsida) and the impact of taxonomic practice and research history on diversity estimates. *Paleobiology* 45(1):1–14 DOI 10.1017/pab.2018.38.
- Pusch LC, Kammerer CF, Fröbisch J. 2019.** Cranial anatomy of the early cynodont *Galesaurus planiceps* and the origin of mammalian endocranial characters. *Journal of Anatomy* 234(5):592–621 DOI 10.1111/joa.12958.
- Pusch LC, Ponstein J, Kammerer CF, Fröbisch J. 2020.** Novel endocranial data on the early therocephalian *Lycosuchus vanderrieti* underpin high character variability in early theriodont evolution. *Frontiers in Ecology and Evolution* 7:464 DOI 10.3389/fevo.2019.00464.
- Rodrigues PG, Ruf I, Schultz CL. 2013.** Digital reconstruction of the otic region and inner ear of the non-mammalian cynodont *Brasilitherium riograndensis* (Late Triassic, Brazil) and its relevance to the evolution of the mammalian ear. *Journal of Mammalian Evolution* 20(4):291–307 DOI 10.1007/s10914-012-9221-2.
- Rodrigues PG, Ruf I, Schultz CL. 2014.** Study of a digital cranial endocast of the nonmammaliaform cynodont *Brasilitherium riograndensis* (Later Triassic, Brazil) and its relevance to the evolution of the mammalian brain. *Paläontologische Zeitschrift* 88:329–352.
- Rodrigues PG, Martinelli AG, Schultz CL, Corfe IJ, Gill AG, Soares MB, Rayfield EJ. 2018.** Digital cranial endocast of *Riograndia guaibensis* (Late Triassic, Brazil) sheds light on the evolution of the brain in non-mammalian cynodonts. *Historical Biology* 31(9):1195–1212 DOI 10.1080/08912963.2018.1427742.

- Ronquist F, Huelsenbeck JP. 2003.** MrBayes 3: Bayesian phylogenetic inference under mixed models. *Bioinformatics* **19**(2):1572–1574 DOI [10.1093/bioinformatics/btg180](https://doi.org/10.1093/bioinformatics/btg180).
- Rowe T, Carlson W, Bortorff W. 1995.** *Thrinaxodon: digital atlas of the skull CD-ROM (Second Edition for Windows and Macintosh platforms)*. Austin, TX: University of Texas Press.
- Seeley HG. 1894.** Researches on the structure, organisation, and classification of the fossil Reptilia. Part IX., Section 1. *Philosophical Transactions of the Royal Society Series B* **185**:987–1018.
- Seeley HG. 1895.** Researches on the structure, organisation, and classification of the fossil Reptilia. Part IX., Section 5. On the Skeleton in New Cynodontia from the Karroo Rocks. *Philosophical Transactions of the Royal Society Series B* **186**:59–148 DOI [10.1098/rstb.1895.0002](https://doi.org/10.1098/rstb.1895.0002).
- Sidor CA, Smith RMH. 2004.** A new galesaurid (Therapsida: Cynodontia) from the Lower Triassic of South Africa. *Palaeontology* **47**(3):535–556 DOI [10.1111/j.0031-0239.2004.00378.x](https://doi.org/10.1111/j.0031-0239.2004.00378.x).
- Sigurdson T. 2006.** New features of the snout and orbit of a therocephalian therapsid from South Africa. *Acta Palaeontologica Polonica* **51**(1):63–75.
- Smith R, Rubidge B, Van der Walt M. 2012.** Therapsid biodiversity patterns and paleoenvironments of the Karoo Basin, South Africa. In: Chinsamy-Turan A, ed. *Forerunners of Mammals: Radiation, Histology, Biology*. Bloomington: Indiana University Press, 31–62.
- Swofford DL. 2003.** *PAUP*. Phylogenetic analysis using parsimony (and other methods)*. Sunderland: Sinauer Associates.
- Tatarinov LP. 1968.** Morphology and systematics of the northern *Dvinia* cynodonts (Reptilia, Therapsida; Upper Permian). *Postilla* **125**:1–51.
- Van den Brandt MJ, Abdala F. 2018.** Cranial morphology and phylogenetic analysis of *Cynosaurus suppostus* (Therapsida, Cynodontia) from the upper Permian of the Karoo Basin, South Africa. *Palaeontologia Africana* **52**:201–221.
- Van Heerden J, Rubidge B. 1990.** The affinities of the early cynodont reptile Nanictosaurus. *Palaeontologia Africana* **27**:41–44.
- Viglietti PA. 2020.** Biostratigraphy of the *Daptocephalus* Assemblage Zone (Beaufort Group, Karoo Supergroup), South Africa. *South African Journal of Geology* **123**(2):191–206 DOI [10.25131/sajg.123.0014](https://doi.org/10.25131/sajg.123.0014).